Progress In Electromagnetics Research M, Vol. 120, 55–67, 2023

A Novel Passive Millimeter Wave Image Noise Suppression Method Based on Pixel Non-Local Self-Similarity

Jin Yang[1, 2] and Yuehua Li[1, *]

Abstract—To solve the problem of mixed noise in a passive millimeter-wave (PMMW) imaging system that affects object detection, recognition, and classification, this paper proposes a blind denoising algorithm based on pixel non-local self-similarity (PNSS) prior to PMMW images. Firstly, an adaptive filtering algorithm is introduced, utilizing PNSS prior to estimating the noise intensity and improving the problem of noise residual caused by parameter uncertainty in traditional filtering processes. Secondly, a three-level joint denoising algorithm is developed, accompanied by an iterative regression algorithm to effectively filter the mixed noise in PMMW images while preserving image contours. Finally, the effectiveness of the proposed method is demonstrated through a comparison with patch similarity-based prior denoising methods and high-dimensional mixed noise denoising methods. Experimental results substantiate that the proposed PNSS blind denoising method successfully suppresses mixed noise in PMMW images, enhances subjective visual perception, and presents a novel approach for denoising under various PMMW imaging mechanisms.

1. INTRODUCTION

Passive Millimeter Wave (PMMW) imaging systems achieve imaging by detecting electromagnetic thermal radiation from natural scenes and utilizing the difference in the energy distribution of millimeter wave radiation between the target scene and the object. Thanks to the ability of millimeter waves to penetrate complex environments such as clouds, smoke, dust, and clothing, PMMW imaging systems can obtain information that is inaccessible to infrared (IR) and optical detection. At the same time, PMMW imaging systems do not actively emit electromagnetic waves, making them highly covert and difficult to detect. Therefore, they are widely used in security imaging, military reconnaissance, and battlefield environment sensing [1–5]. However, practical PMMW images often suffer from severe noise, low resolution, and blurring compared to IR and optical images. These issues arise from factors such as antenna aperture size, diffraction effects, and partial coherence between targets, making it challenging to identify targets effectively from the scene [2]. Therefore, noise suppression is one of the critical challenges for PMMW imaging systems.

Currently, there are two main research focuses on PMMW image denoising. One approach involves modifying the inversion algorithm for different imaging mechanisms [6–10], while the other aims to improve image quality based on image features [2, 11–13]. For instance, an adaptive reconstruction method has been proposed for the total-power radiometer imaging mechanism [8]. This method operates directly on the raw samples from the sensor and constructs each pixel via a smoothing Kernel, resulting in improved contrast and reduced noise. Another approach is the adaptive clean algorithm proposed in [9], which corrects the magnitude of the target and selects a matching point spread function (PSF) based on the azimuth of the target. This method enhances the information of the target in the near-field

Received 7 September 2023, Accepted 16 October 2023, Scheduled 22 October 2023
* Corresponding author: Yuehua Li (nlglyh2013@sina.cn).
[1] School of Electronic Engineering and Optoelectronic Technology, Nanjing University of Science and Technology, Nanjing 210094, China. [2] Huaian Key Laboratory of Millimeter-Wave Communication Technology, Huaiyin Normal University, Huaian 223300, China.

synthetic aperture imaging mechanism. Additionally, a real-time calibration method for the visibility function of millimeter-wave passive imaging has been proposed in [10]. This method effectively corrects the additive error of the visibility function and is applied to the hybrid structure composed of a phased array and synthetic aperture. However, these methods are specific to certain imaging mechanisms and lack generalization. Therefore, there is a need to enhance PMMW image quality based on image features.

Previous studies have shown that the non-local self-similarity (NSS) prior approach is advantageous for improving image quality [14, 15]. Building upon the patch non-local self-similarity prior theory, previous works [11, 12] have improved Non-local Means (NLM) and Block-Matching and 3D filtering (BM3D) algorithms to suppress Gaussian noise in PMMW images. These methods have some improvements for PMMW images. However, in the actual imaging process of the PMMW imaging system, in addition to thermal noise, there is impulsive noise caused by uneven power density and strip noise caused by channel inconsistency and antenna baseline position errors. Therefore, it is necessary to suppress impulse noise and strip noise while filtering out thermal noise. Considering that the pixel is the smallest component of a natural image, the NSS prior can be extended from the patch level to the pixel level. Previous works [16–19] have demonstrated the effectiveness of using pixel non-local self-similarity (PNSS) and proposed the non-local Haar (NLH) algorithm that achieves superior denoising performance on real-world quasi-Gaussian noise images and remains competitive with state-of-the-art deep learning methods [16]. In this paper, we extend the concept of PNSS to PMMW image restoration and propose a three-level joint denoising algorithm based on PNSS. Experimental results show that our proposed method effectively improves the quality of PMMW images and enhances subjective visual perception. In summary, our major contributions are manifold:

(i) We introduce the theory of pixel non-local self-similarity for preprocessing PMMW images. Based on the PNSS prior, and we accurately estimate the noise level and propose a novel blind denoising method to remove noise from PMMW images.

(ii) In the process of suppressing mixed noise, we propose a three-level joint denoising model and utilize an iterative regression algorithm to effectively eliminate mixed noise in PMMW images while preserving image texture and contours.

(iii) Experimental results on optical images and real PMMW images demonstrate that our proposed method outperforms traditional methods in terms of performance.

(iv) This research provides a new technique for reducing mixed noise in PMMW images obtained from all imaging mechanisms.

The rest of this paper is organized as follows. Section 2 introduces the theory of pixel non-locally self-similarity. Section 3 provides a detailed description of the mixed noise filtering algorithm. Section 4 presents simulation results for optical and PMMW images. Finally, Section 5 concludes this paper.

2. PIXEL NON-LOCAL SELF-SIMILARITY THEORY

Non-local self-similarity is the essence of successfully achieving image denoising. Both the classical NLM and BM3D algorithms utilize patch-level self-similar priors for denoising [14, 15] while ignoring their intra-patch variance. As the smallest element in a natural image, pixels also exhibit certain similarities among different pixels within the same patch. Therefore, in addition to searching for similar patches, further exploration of similar pixels can facilitate a priori denoising at the pixel level.

The search for non-local similar pixels first necessitates finding non-local similar patches. Subsequently, each similar patch is reshaped into a column vector, and the column vectors of all similar patches are aggregated into a similar patch matrix. For each row of pixels, situated at the same position of different patches, the patch-level non-local prior ensures that the pixels in the same row are similar to a certain degree. Finally, as suggested by [16], we calculate the Euclidean distance between different rows to measure pixel similarity. We select the rows with the closest similar pixels to form a similar patch matrix. For a noisy image, Table 1 illustrates the process of searching for similar pixels.

Table 1. Searching non-local similar pixels.

Input: $y_{\mathrm{n}} \in \mathbb{R}^{a\times b}$ (PMMW reconstruction image)

1) Extract local patches

Partitioning the PMMW image y_{n} into interlocking local patches $y_l \in \mathbb{R}^{w\times w}$, $l \in (1,\cdots,Y)$.

(Assume there are total Y patches, the size of each local patch is $w \times w$.)

2) Search similar patches

For a reference patch $y_{l,i}$, we calculate Euclidean distance $\mathrm{D}_{l,ij}$ between $y_{l,i}$ and $y_{l,j}$(other patches in a window of size $C \times C$ around $y_{l,i}$) as

$$\mathrm{D}_{l,ij} = \|y_{l,i} - y_{l,j}\|_2. \tag{1}$$

Select $d-1$ most similar patches and stretch each local patch as a column vector $w \times w \to w^2 \times 1$.

Stack the d most similar patches (including itself) column by column to form a noisy patch matrix as

$$Y_l = [y_{l,1},\ldots,y_{l,d}] = \begin{pmatrix} y_l^{1,1} & \cdots & y_l^{1,d} \\ \vdots & \ddots & \vdots \\ y_l^{w^2,1} & \cdots & y_l^{w^2,d} \end{pmatrix} \in \mathbb{R}^{w^2\times d}. \tag{2}$$

3) Search similar pixels

For the $i-th$ row $y_l^i, i \in \left(1,\ldots w^2\right)$, we calculate the Euclidean distances d_l^{ij} between y_l^i and y_l^j(other rows in Y_l) as

$$\mathrm{d}_l^{ij} = \left\|y_l^i - y_l^j\right\|_2. \tag{3}$$

Select g rows with the smallest distance in Y_l and aggregate them as a pixel similarity matrix:

$$Y_l^{ig} = \begin{pmatrix} y_l^{i_1,1} & \cdots & y_l^{i_1,d} \\ \vdots & \ddots & \vdots \\ y_l^{i_g,1} & \cdots & y_l^{i_g,d} \end{pmatrix} \in \mathbb{R}^{g\times d}, \tag{4}$$

where $\{i_1,\ldots,i_g\} \subset \left\{1,\ldots,w^2\right\}$,$i \in \left(1,\cdots,w^2\right)$,$l \in (1,\cdots,Y)$.

4) Repeating 3) to find all similarity matrices in Y_l.

5) Repeating 2) and 3) to find all similarity matrices for Y patches.

Omit index i, the pixel similarity matrix is abbreviated as Y_l^g.

Output: $Y_l^g \in \mathbb{R}^{g\times d}$ (the pixel similarity matrix)

3. THE PROPOSED METHOD

In this section, we introduce our proposed Pixel Non-local Self-Similarity (PNSS)-based method for blind denoising of PMMW images. The method consists of three parts: 1) Noise and signal intensity estimation (Section 3.1), 2) Harr Transform domain Wiener soft threshold denoising and adaptive median filtering (Section 3.2), and 3) Edge enhancement (Section 3.3). The structure of the method is illustrated in Fig. 1.

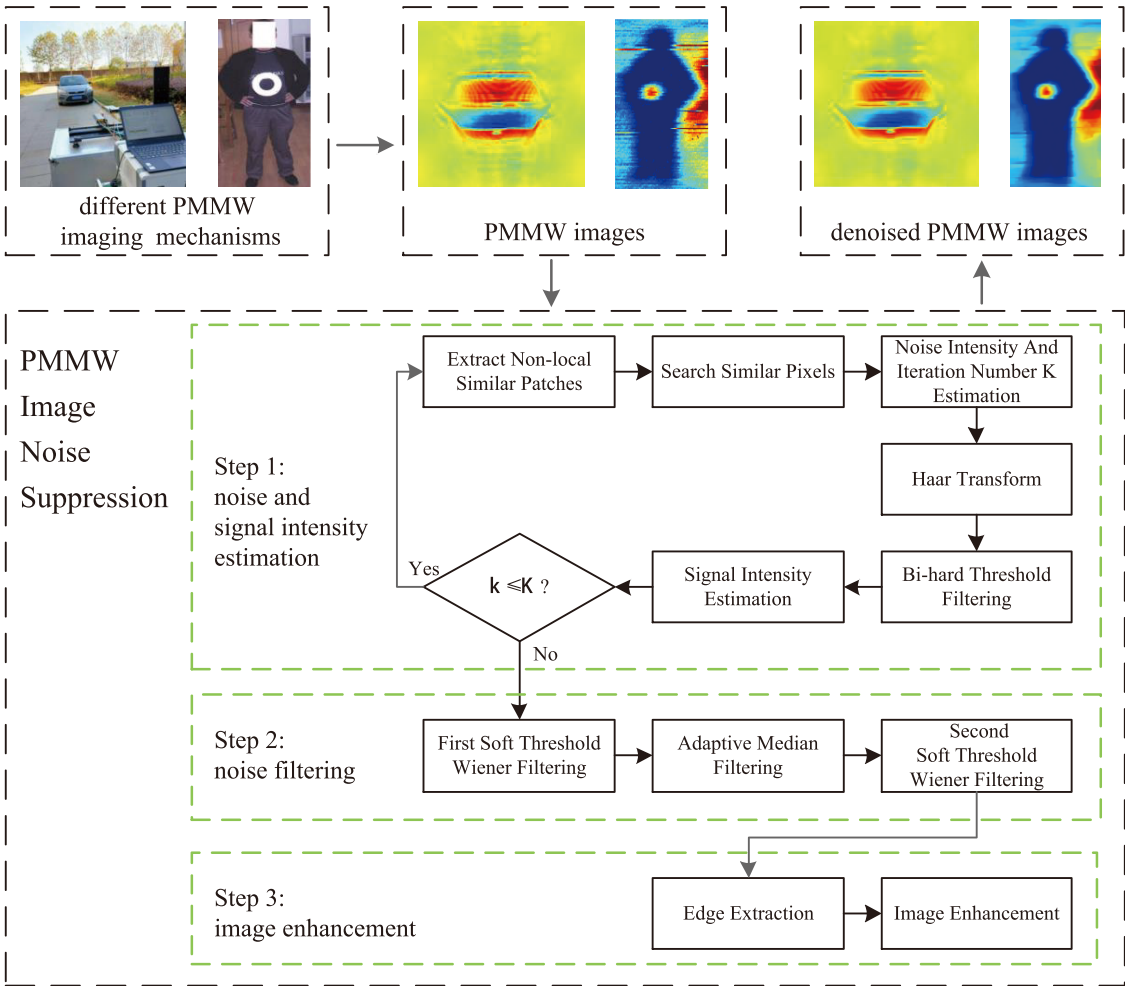

Figure 1. The structure diagram of PMMW image mixed noise suppression.

3.1. Noise Level and Signal Intensity Estimation

3.1.1. Noise Level Estimation

Accurate noise estimation can enhance the precision of various filtering parameters, enabling blind denoising. Given that the selected g rows of pixels in the pixel similarity matrix are very similar, we use the standard deviation of the Euclidean distance between g rows to calculate local noise intensity:

$$\sigma_l = \frac{1}{w^2\,(g-1)} \sum_{j=2}^{g} \sum_{i=1}^{w^2} \sqrt{\frac{1}{d}\left(d_l^{ij}\right)^2}. \tag{5}$$

To increase method robustness, we expand noise level estimation from local to global. We estimate the local noise level for all noisy similar pixel matrices in the image and set the global noise intensity as the mean of local noise intensities:

$$\sigma_g = \frac{1}{Y} \sum_{l=1}^{Y} \sigma_l. \tag{6}$$

In strongly textured regions, distinguishing between signal and noise is challenging, leading to possible overestimation of noise intensity. To address this, we sort local noise estimates from smallest

to largest, discard the maximum local noise intensity, and calculate the modified global noise level as

$$\hat{\sigma}_g = \frac{1}{Y-1}\sum_{l=1}^{Y-1}\hat{\sigma}_l, \tag{7}$$

where $\hat{\sigma}_l$ is the sorted local noise intensities.

3.1.2. Local Signal Intensity Estimation

Estimating signal intensity is critical for determining subsequent Wiener filter coefficients. We achieve simple signal intensity estimation through two-stage hard threshold denoising in the Haar transform domain. First, we apply the Lifting Haar Wavelet Transform (LHWT) on the pixel similarity matrix to generate a noise coefficient matrix as

$$C_l^g = T\left(Y_l^g\right), \tag{8}$$

where $T(\,)$ denotes the orthogonal LHWT.

We then perform the first hard threshold filtering on the noise coefficient matrix via

$$\hat{C}_l^g(i,j) = \begin{cases} C_l^g(i,j) & C_l^g(i,j) \geq |\mu_y - m_y|\,\hat{\sigma}_g^2 \\ 0 & C_l^g(i,j) < |\mu_y - m_y|\,\hat{\sigma}_g^2 \end{cases}, \tag{9}$$

where μ_y and m_y represent the mean and median pixel intensities of Y_l^g, and $i \in (1,\cdots,g)$, $j \in (1,\cdots,d)$ denote the row and column indices of $\hat{C}_l^q$.

According to wavelet theory, the coefficients of the last two rows (excluding the first column) of the noise coefficient matrix fall within the high-frequency band [20], which is likely noise and should be filtered out. To this end, we perform a second hard threshold filtering via

$$\tilde{C}_l^g(i,j) = \begin{cases} \hat{C}_l^g(i,j) & \\ 0 & (i = g-1, g)\,\&\,(j \neq 1) \end{cases}. \tag{10}$$

We approximate the filtered noise coefficient matrix as the local signal intensity. To better retain detail information, we adopt the concept of iterative regression and obtain the noisy image $y_{(k)_n}$ as

$$y_{(k)_n} = \alpha y_{(k-1)_n} + (1-\alpha)\,y_n, \tag{11}$$

where $k \in (1,\cdots,K)$, and α is the iteration coefficient.

3.2. Mixed Noise Suppression

This section details three stages of blind PMMW image denoising using Wiener filtering and median filter. Initially, we apply Wiener soft threshold blind denoising on the noise coefficient matrix in the Haar transform domain. We construct the Wiener filter coefficients using the previously estimated signal intensity in (10) and noise intensity in (7), and perform Wiener filtering on C_l^g in (8):

$$\overline{C}_l^g = \frac{\left|\tilde{C}_l^g\right|^2}{\left|\tilde{C}_l^g\right|^2 + \hat{\sigma}_g^2}\, C_l^g. \tag{12}$$

Then, we perform the inverse LHWT on the filtered coefficient matrix to obtain the denoised pixel matrices via

$$\overline{Y}_l^g = T^{-1}\left(\overline{C}_l^g\right), \tag{13}$$

where $T^{-1}(\cdots)$ denotes the inverse LHWT.

We aggregate all the denoised pixel matrices to create the denoised image $\overline{y}_n$.

On analyzing the nature of Wiener filtering, we observe its notable denoising effect on thermal noise with statistical regularity. However, due to the existence of mixed noise, impulse noise and strip noise still persist after Wiener filtering. To effectively remove the mixed noise in the PMMW images,

we opt for the median filter, which possesses a significant filtering effect on impulse noise. In traditional median filtering, the fixed size of the filter window often limits the denoising effect under severe noise pollution. To enhance the denoising effect, we automatically adjust the filter window W based on global noise intensity and perform the modified median filter as

$$\overline{\overline{y}}_n = med\left\{\overline{y}_n\left(i-m, j-n\right), (m,n \in W)\right\}. \tag{14}$$

In order to maintain image details, the Wiener soft threshold filtering utilized in (12) specifically targets the noise coefficient matrices C_l^g of the original noisy image y_n. It does not operate on the coefficients of the denoised image $y_{(k)_n}$ obtained after two-stage hard-threshold filtering. Therefore, some noise residue is typically left after Wiener and median filtering. To achieve a superior denoising outcome, we perform a second Wiener soft threshold filtering as

$$\breve{C}_l^g = \frac{\left|\tilde{C}_l^g\right|^2}{\left|\tilde{C}_l^g\right|^2 + \hat{\sigma}_g^2}\overline{\overline{C}}_l^g, \tag{15}$$

where $\overline{\overline{C}}_l^g$ is the noise coefficient of $\overline{\overline{y}}_n$ which has been preprocessed with median filtering and a preliminary Wiener filter.

We obtain the denoised pixel matrix $\breve{y}_l^g$ by performing inverse LHWT transforms for $\breve{C}_l^g$. Lastly, we aggregate all the denoised pixel matrices to form the final denoised image $\breve{y}$.

3.3. Edge Enhancement

After three stages of denoising, the mixed noise is removed while the contour information is blurred. For PMMW images with less texture, contour information is the key to PMMW image processing compared with enhancing texture information. As the edge in the basic denoised image $\breve{y}$ is still blurry, and some serious noise has not been removed completely, we perform an enhancement algorithm based on the Laplacian of Gaussian (LoG) operator as follows:

$$\breve{y}_{\log} = \breve{y} + \breve{y} * \nabla^2 G, \tag{16}$$

$$\nabla^2 G = \frac{\partial^2 G}{\partial x^2} + \frac{\partial^2 G}{\partial y^2} = \frac{1}{2\pi {\sigma_{LoG}}^4}\left(\frac{x^2+y^2}{{\sigma_{LoG}}^2} - 2\right) e^{-\frac{x^2+y^2}{2{\sigma_{LoG}}^2}}, \tag{17}$$

where σ_{LoG} is the Gauss standard deviation.

3.4. Complexity Analysis

The proposed method contains three steps: 1) in Section 3.1, the complexity of patch matching is $\mathcal{O}(\mathrm{abC}^2w^2)$, while the complexity of pixel matching is $\mathcal{O}(\mathrm{ab}dw^4)$; the complexity of noise estimation is $\mathcal{O}(\mathrm{ab}gw^2)$; and the complexity of signal intensity estimation based on LHWT is $\mathcal{O}(\mathrm{ab}gdw^2)$. Since the above process iterates K times, the complexity of Section 3.1 is $\mathcal{O}(\mathrm{ab}Kw^2 * \max(C^2, dw^2, gd))$; 2) in Section 3.2, the complexity of Wiener soft threshold filtering is $\mathcal{O}(\mathrm{ab}dw^2)$, and the complexity of adaptive median filtering is $\mathcal{O}(\mathrm{ab}W\log(W))$; 3) in Section 3.3, the complexity of image enhancement is $\mathcal{O}(\mathrm{ab}W^2)$. Since we have $C > W, C^2 > gd$, the first step has the highest complexity, and the complexity of our method is $\mathcal{O}(\mathrm{ab}Kw^2 * \max(C^2, dw^2))$.

4. EXPERIMENTAL RESULTS AND DISCUSSIONS

In this section, we conduct experiments on multiple images to verify the effectiveness of the proposed filtering algorithm. (1) Optical images: Select two classic digital images (Lena, Pepper), which are affected by varying standard deviations of Gaussian noise and different probabilities of impulse noise. (2) Real PMMW images: Real PMMW images were acquired using different mechanisms (Dicke Radiometer Imaging System, Interferometric Synthetic Aperture Radiometer Imaging System) in the 3 mm band.

4.1. Implementation Details

All following experiments are done under the MATLAB r2020a environment. The proposed method includes 8 main parameters, where patch size is w; number of similar patches is d; number of similar pixel rows is g; the Gauss standard deviation is σ_{LoG}; window size for searching similar patches is C; regularization parameter is α; iteration number is K; and the median filter window is W. We set $\alpha = 0.408$, $K = 4$ for $0 < \hat{\sigma}_g \leq 30$, $\alpha = 0.618$, $K = 3$ for $\hat{\sigma}_g > 30$, $W = 3 \times 3$ for $0 < \hat{\sigma}_g \leq 60$, and $W = 5 \times 5$ for $\hat{\sigma}_g > 60$. In order to perform Haar transform, d and g should be set to powers of 2. Since searching for too many pixels or patches may reduce the accuracy of non-local self-similarity, we set $d = 16$ and $g = 4$ as suggested by [16]. The performance increases with the increase of patch size w and window size C. To achieve a balance between performance and speed, we set $w = 10$ and $C = 40$. The details of other parameters are set as shown in Table 2.

Table 2. Parameters of our proposed method.

Parameter		w	d	g	σ_{LoG}	C	α	K	W
Value	$0 < \hat{\sigma}_g \leq 30$	10	16	4	1.6	40	0.408	4	3×3
	$30 < \hat{\sigma}_g \leq 60$						0.618	3	3×3
	$\hat{\sigma}_g > 60$						0.618	3	5×5

The Peak Signal-to-Noise Ratio (PSNR) and Structural Similarity Index Measurement (SSIM) [21] are used as objective evaluation criteria to evaluate the performance of the proposed methods. In evaluating PMMW images, due to the lack of ground truth PMMW images, we adopt the method noise [14] proposed by Buades et al. as a subjective evaluation criterion for indirectly judging the effectiveness of the denoising algorithm. The method noise represents the information filtered out during image processing and can be defined as

$$n(D_h, u) = u - D_h(u), \tag{18}$$

where u is the noisy image, and D_h is the filtering operator.

Moreover, the different methods include Non-local Means (NLM), Block-Matching and 3D (BM3D), Mean Filtering (MF), Non-local Haar (NLH), Adaptive Manifolds High-dimensional Mean Median Filter (AM-HMF) which are used to compare their performance with that of the proposed algorithm.

4.2. Experiments on Optical Images

The first experiment was performed on the standard images corrupted with different noise levels. Table 3 summarizes the PSNR and SSIM scores of the denoising obtained by some representative state-of-the-art methods on the optical images. The best results are highlighted in bold. Furthermore, Fig. 2 shows the trend of PSNR and SSIM with noise intensity.

It is evident that PSNR and SSIM values of the six algorithms tend to decrease with increasing noise intensity, indicating a decline in algorithm performance. The MF algorithm operates inconsistently, effectively removing noise at low levels but experiencing a significant performance drop with increased noise intensity. On the other hand, the denoising capabilities of the BM3D and NLH algorithms remain relatively stable, with PSNR and SSIM values initially decreasing and then increasing with higher noise intensity. This can be attributed to their superior denoising abilities for Gaussian noise. However, these benefits are compromised when dealing with mixed noise, particularly noticeable in the NLH algorithm. Meanwhile, the NLM and AM-HMF algorithms exhibit a stepwise degradation in performance as the noise intensity increases. This degradation is primarily caused by the noise component dominating the image, making it progressively more challenging to restore the original image. Despite the adverse effects of strong noise on image denoising, the algorithm proposed in this study consistently outperforms the others. Its denoising performance for mixed noise is not limited to a specific noise intensity level.

Figures 3 and 4 display the qualitative results of the visual quality of the six methods. Due to space limitations, here we present the denoising results for the weak and strong noise cases. As observed in

Table 3. Quantitative results (PSNR and SSIM) of a comparative study on the optical images.

Noise level	Lena						Pepper					
Std (σ)	10	20	30	40	50	60	10	20	30	40	50	60
Probability(%)	1	2	3	4	5	6	1	2	3	4	5	6
PSNR comparison (dB)												
MF	31.29	27.91	25.17	22.97	21.16	19.64	30.76	27.61	25.00	22.86	21.10	19.62
NLM	28.51	26.60	25.87	25.20	24.21	23.21	27.76	25.95	25.42	24.88	23.87	22.77
BM3D	27.43	27.58	27.67	27.05	26.77	25.56	26.61	26.64	26.76	26.12	25.38	24.11
NLH	25.33	23.50	23.96	24.41	24.84	24.70	25.24	23.50	23.96	24.41	24.84	24.70
AM-HMF	29.94	29.15	28.26	27.39	25.58	22.84	29.47	28.68	27.29	26.30	24.88	22.95
The proposed	**33.03**	**31.22**	**29.84**	**28.59**	**27.48**	**26.51**	**32.14**	**30.54**	**29.19**	**27.99**	**26.89**	**25.90**
SSIM comparison												
MF	0.979	0.958	0.925	0.884	0.836	0.784	0.978	0.957	0.926	0.888	0.844	0.798
NLM	0.966	0.947	0.935	0.925	0.908	0.888	0.960	0.942	0.932	0.921	0.904	0.884
BM3D	0.956	0.955	0.957	0.953	0.953	0.943	0.951	0.946	0.945	0.940	0.934	0.921
NLH	0.934	0.900	0.904	0.912	0.921	0.921	0.933	0.895	0.897	0.898	0.902	0.899
AM-HMF	0.975	0.971	0.965	0.958	0.937	0.885	0.972	0.966	0.954	0.944	0.925	0.888
The proposed	**0.986**	**0.980**	**0.973**	**0.966**	**0.957**	**0.949**	**0.983**	**0.976**	**0.967**	**0.957**	**0.948**	**0.938**

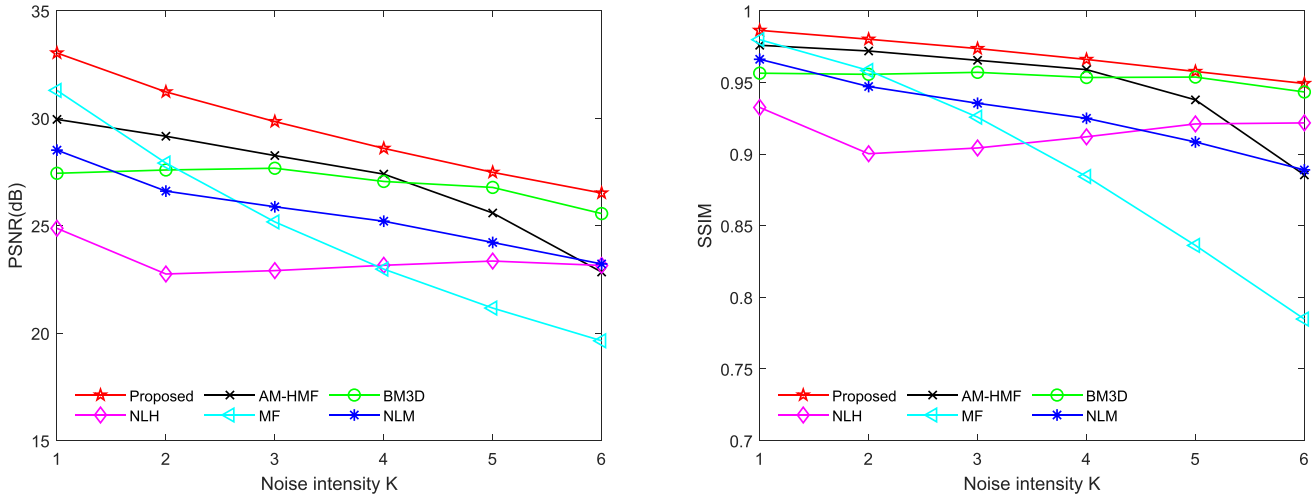

Figure 2. Comparison of performance between six methods for Lena image. (a) PSNR, (b) SSIM.

Fig. 3, the NLM, BM3D, and NLH methods successfully reduce Gaussian noise in weak noise images, but struggle to filter impulse noise effectively. In contrast, the MF method effectively eliminates impulse noise while retaining Gaussian noise. The AM-HMF method, utilizing a high-dimensional mean median filter and adaptive manifolds, exhibits the capability to address most noise but results in blurred image details and edges. Our method employing a three-stage blind denoising algorithm, effectively removes

Figure 3. The performance of six methods for Lena image with weak noise ($\sigma = 20$, Probability $= 2\%$). (a) Original image, (b) noisy image, (c) denoised by NLM, (d) denoised by BM3D, (e) denoised by MF, (f) denoised by NLH, (g) denoised by AM-HMF, (h) denoised by the proposed method.

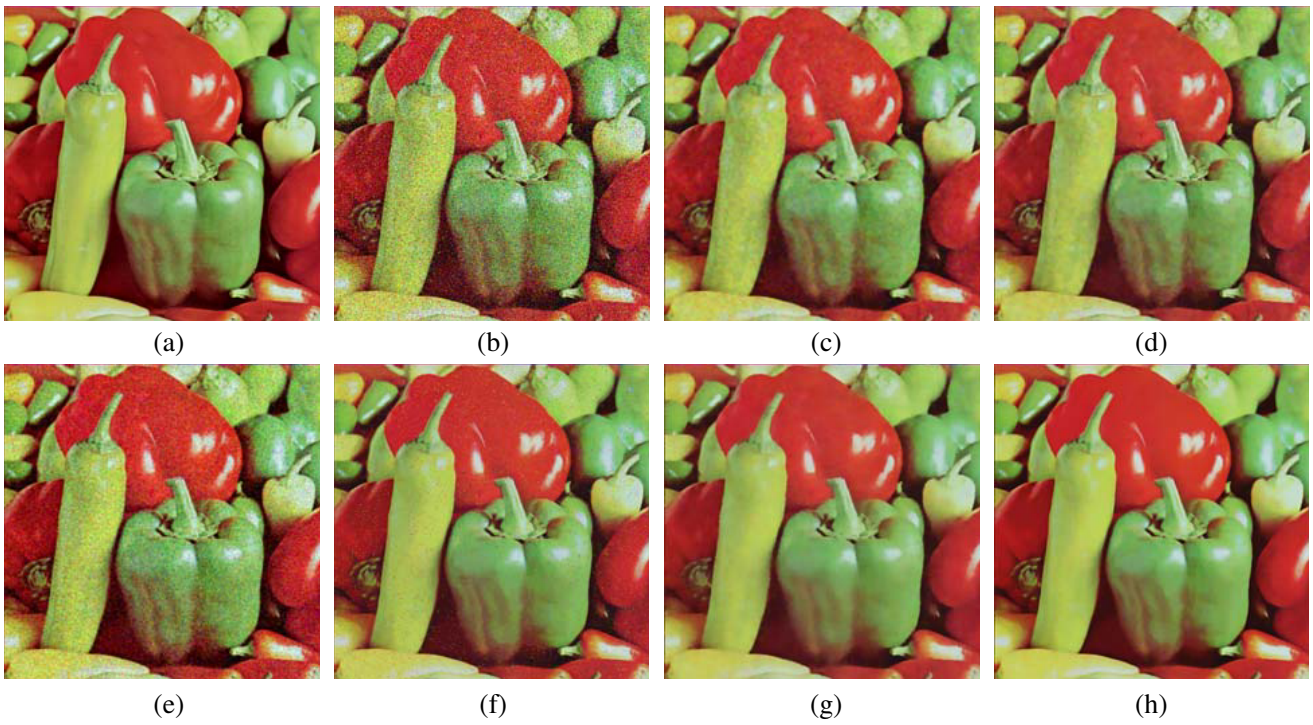

Figure 4. The performance of six methods for Pepper image with strong noise ($\sigma = 40$, Probability $=$ 4%). (a) Original image, (b) noisy image, (c) denoised by NLM, (d) denoised by BM3D, (e) denoised by MF, (f) denoised by NLH, (g) denoised by AM-HMF, (h) denoised by the proposed method.

most of noise and yields the most favorable denoising outcomes. Moving on to the strong noise image presented in Fig. 4, the MF method fails to sufficiently eliminate most noise, resulting in unsatisfactory results. The NLM and BM3D methods perform better than MF, but the outcomes are still suboptimal. NLH, despite its proficiency in reducing Gaussian noise, retains more impulse noise. The denoised image appears overly smoothed with the AM-HMF method. In contrast, our method achieves greater effectiveness by removing most noise while preserving edge and structural information.

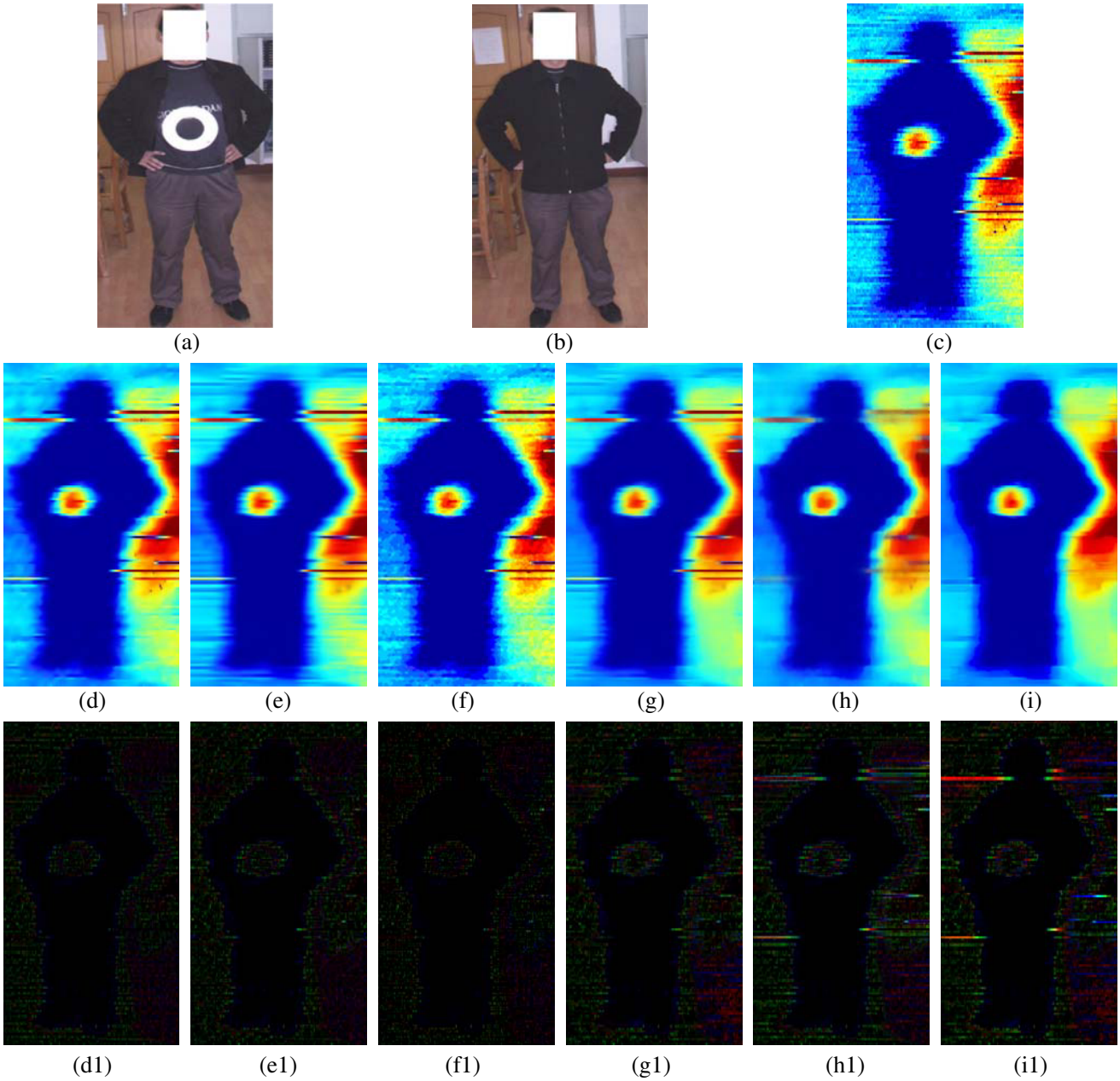

Figure 5. The performance of the proposed algorithm for real PMMW images obtained by the Dicke radiometer imaging system. (a) Reference scene, (b) target scene, (c) real PMMW image, (d) denoised by NLM, (e) denoised by BM3D, (f) denoised by MF, (g) denoised by NLH, (h) denoised by AM-HMF, (i) denoised by the proposed method, (d1)–(i1) the corresponding method noise of different methods.

4.3. Experiments on Real PMMW Images

The second experiment was performed on Real PMMW Images acquired through various imaging mechanisms. Fig. 5 and Fig. 6 demonstrate the performance of our denoising method.

The visual quality results of the six methods for PMMW images and the corresponding method noise are displayed in Fig. 5. As shown in Fig. 5, the MF method denoises poorly and retains most of the noise. In contrast, the NLM, BM3D, and NLH methods successfully reduce most of the noise in the PMMW image, but filtering effectiveness is limited for stripe noise and strong noise points. The AM-HMF method is more effective, but there is still residual noise, and the edge blurring is obvious. The proposed method effectively eliminates most noise in the PMMW image while preserving edges. Furthermore, we have successfully identified a metal ring (Fig. 5(i)), the structure of an automobile (Fig. 6(d1)), semi-concealed metal disk (Fig. 6(d2)), and distant heater (Fig. 6(d3)) in the denoised images, rendering our method useful for specialized engineering applications, such as target identification, security imaging,

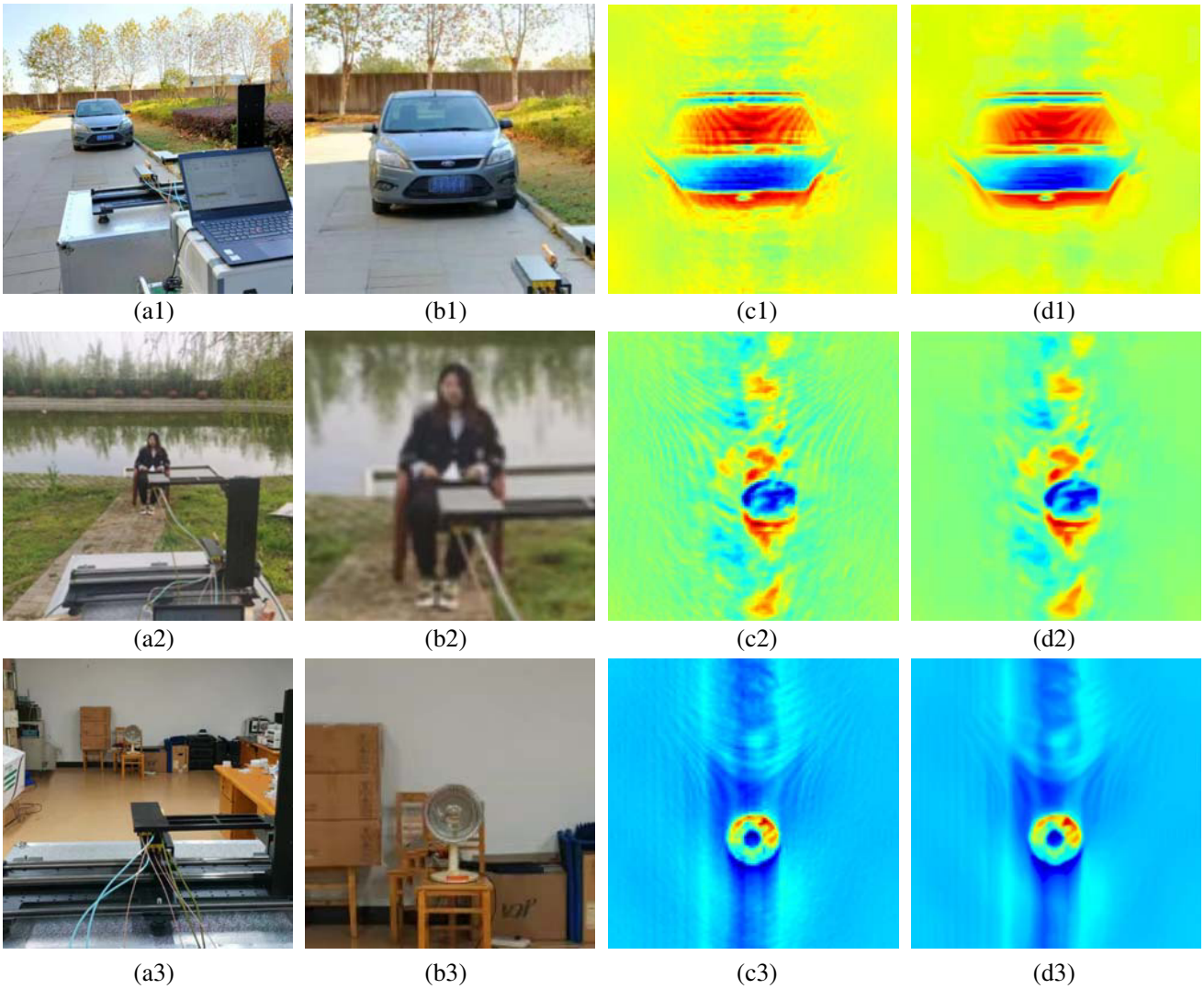

Figure 6. The performance of the proposed algorithm for real PMMW images obtained by interferometric synthetic aperture radiometer imaging system. (a1) Reference scene: car at a distance of 6 m, (a2) reference scene: human carrying semi-concealed metal disk at a distance of 3.3 m, (a3) reference scene: heater at a distance of 5 m, (b1)–(b3) the corresponding target scene, (c1)–(c3) the corresponding real PMMW images, (d1)–(d3) the corresponding denoised images by our method.

and military reconnaissance. Therefore, our proposed method is practical and efficient for working with real PMMW images.

5. CONCLUSIONS

This paper proposes a blind filtering algorithm based on pixel non-local self-similarity for mixed noise in PMMW images. The algorithm performs the Haar transform on the pixel similarity matrix, achieving a better combination of pixel self-similarity prior and transform domain methods. The introduced noise and signal intensity estimation methods provide effective parameter estimation for subsequent blind filtering. The proposed three-stage filtering model effectively suppresses mixed noise, and target edges are enhanced using an image enhancement algorithm based on the Laplace Gaussian operator. Experimental results demonstrate that the proposed filtering algorithm can filter out the mixed noise of PMMW images and outline the target structure, providing a reference for the blind filtering of mixed noise in PMMW images under various imaging mechanisms.

REFERENCES

1. Chen, J., Y. Li, J. Wang, Y. Li, and Y. Zhang, "An accurate imaging algorithm for millimeter wave synthetic aperture imaging radiometer in near-field," *Progress In Electromagnetics Research*, Vol. 141, 517–535, 2013.
2. Zhu, S., Y. Li, J. Chen, and Y. Li, "Passive millimeter wave image denoising based on adaptive manifolds," *Progress In Electromagnetics Research B*, Vol. 57, 63–73, 2014.
3. Cheng, Y., Y. Wang, Y. Niu, H. Rutt, and Z. Zhao, "Physically based object contour edge display using adjustable linear polarization ratio for passive millimeter-wave security imaging," *IEEE Transactions on Geoscience and Remote Sensing*, 1–15, 2020.
4. Peng, R., J. Chen, Z. Liu, and Z. Guo, "Millimeter wave image super resolution using multichannel depth convolution neural network," *Progress In Electromagnetics Research M*, Vol. 113, 225–235, 2022.
5. Yang, H., Z. Yang, A. Hu, C. Liu, T. J. Cui, and J. Miao, "Source-free domain adaptive detection of concealed objects in passive millimeter-wave images," *IEEE Transactions on Instrumentation and Measurement*, Vol. 72, No. 5005015, 1–15, 2023.
6. Fu, P., D. Zhu, F. Hu, Y. Xu, and H. Xia, "A near-field imaging algorithm based on angular spectrum theory for synthetic aperture interferometric radiometer," *IEEE Transactions on Microwave Theory and Techniques*, Vol. 70, No. 7, 3606–3616, 2022.
7. Sun, D., Y. Shi, and Y. Feng, "Blind deblurring and denoising via a learning deep CNN denoiser prior and an adaptive L0-regularised gradient prior for passive millimetre-wave images," *IET Image Processing*, Vol. 14, No. 17, 4774–4784, 2020.
8. Sarkis, M., "Adaptive reconstruction of millimeter-wave radiometric images," *IEEE Transactions on Image Processing*, Vol. 21, No. 9, 4141–4151, 2012.
9. Chen, J., Y. Li, J. Wang, Y. Li, and Y. Zhang, "Adaptive CLEAN algorithm for millimeter wave synthetic aperture imaging radiometer in near field," *IET Image Processing*, Vol. 9, No. 3, 218–225, 2015.
10. Zhao, Y., W. Si, A. Hu, and J. Miao, "A real-time calibration method of visibility function for passive millimeter wave imaging," *IEEE International Conference on Microwave and Millimeter Wave Technology*, 2020.
11. Li, Y. and Y. Li, "Passive millimeter-wave image denoising based on improved algorithm of non-local mean," *International Journal of Advancements in Computing Technology*, Vol. 4, No. 10, 158–164, 2012.
12. Li, Y., Y. Li, H. Su, Z. Li, and S. Zhu, "Passive millimeter wave image denoising based on improved version of BM3D," *Advances in Information Sciences & Service Sciences*, Vol. 4, No. 22, 106–113, 2012.

13. Zhu, S., Y. Li, and Y. Li, "A PMMW image denoising based on adaptive manifolds and high-dimensional mean median filter," *Optik*, Vol. 126, No. 24, 5624–5628, 2015.
14. Buades, A., B. Coll, and J. M. Morel, "A non-local algorithm for image denoising," *IEEE Computer Society Conference on Computer Vision and Pattern Recognition*, Vol. 2, 60–65, 2005.
15. Dabov, K., A. Foi, V. Katkovnik, and K. Egiazarian, "Image denoising by sparse 3-D transform-domain collaborative filtering," *IEEE Transactions on Image Processing*, Vol. 16, No. 8, 2080–2095, 2007.
16. Hou, Y., J. Xu, M. Liu, G. Liu, L. Liu, F. Zhu, and L. Shao, "NLH: A blind pixel-level non-local method for real-world image denoising," *IEEE Transactions on Image Processing*, Vol. 29, 5121–5135, 2020.
17. Hou, H., Y. Shao, Y. Geng, Y. Hou, P. Ding, and B. Wei, "PNCS: Pixel-level non-local method based compressed sensing undersampled MRI image reconstruction," *IEEE Access*, Vol. 11, 42389–42402, 2023.
18. Xu, J., Z.-A. Liu, Y.-K. Hou, X.-T. Zhen, L. Shao, and M.-M. Cheng, "Pixel-level non-local image smoothing with objective evaluation," *IEEE Transactions on Multimedia*, Vol. 23, 4065–4078, 2021.
19. Zhu, R., X. Li, Y. Wang, and X. Zhang, "Medical image fusion based on pixel-level nonlocal self-similarity prior and optimization," *International Conference on Database Systems for Advanced Applications*, 2022.
20. Sweldens, W., "The lifting scheme: A custom-design construction of biorthogonal wavelets," *Applied and Computational Harmonic Analysis*, Vol. 3, No. 2, 186–200, 1996.
21. Wang, Z., A. C. Bovik, H. R. Sheikh, and E. P. Simoncelli, "Image quality assessment: From error visibility to structural similarity," *IEEE Transactions on Image Processing*, Vol. 13, No. 4, 600–612, 2004.